International Journal of Coal Science & Technology (2024) 11:68
https://doi.org/10.1007/s40789-024-00719-4

RESEARCH

Investigation of ground subsidence response to an unconventional longwall panel layout

Pengfei Wang[1] · Zhuang Zhu[1] · Linfeng Guo[2] · Huixian Wang[1] · Yue Qu[3] · Yaoxiong Zhang[4] · Linwei Wang[5] · Hua Wang[6]

Received: 10 October 2023 / Revised: 10 April 2024 / Accepted: 3 July 2024

Abstract
Ground subsidence caused by extraction of longwall panels has always been a great concern all over the world. Conventional longwall mining system (CLMS) gives rise to wavy subsidence causing great damage to surface structures. A coal mine in Shanxi, China, utilizes a split-level longwall layout (SLL) for a sub-horizontal No. 8 coal seam to improve the cavability of mudstone interlayer and top coal. This layout, however, also produced unexpectedly favorable surface subsidence. Subsidence of No. 6 and No. 8 longwall panels was monitored while mining was conducted. Field instrumentation and numerical simulation were carried out. It is demonstrated that an asymmetric subsidence profile with stepped subsidence and cracks occurred on the tailgate side but relatively mild and smooth deformation on the other. Due to elimination of conventional parallelepiped gate pillar, No. 6 and No. 8 gobs were connected. Extraction of two SLL panels acted as one supercritical panel. The maximum possible subsidence was reached which lowers the likelihood of potential future secondary subsidence as underground gob fractures and voids have closed. Therefore, SLL is more favorable for post-mining land reuse as gobs are more consolidated underground.

Keywords Ground subsidence · Longwall mining · Split-level · Mudstone interlayer · Green mining

1 Introduction

Mining subsidence is a depression caused by extraction of mineral deposits from underground (Peng et al. 1992; Lee et al. 2013; Sahu and Lokhande 2015; Maria et al. 2022; Malinowska et al. 2022). Longwall mining is a commonly used underground mining technique with high efficiency and productivity (Peng 2006). It is increasingly popular all over the world for extraction of coal, trona, potash, etc. A longwall mining system typically has one or more gates or entries approximately 150 to 400 m apart, providing an interconnection and then mining the rib of the interconnection on a longwall: hence the name, longwall mining. With the simplest mining system, continuous production and full automation potential, it can further enhance productivity, safety and health of the underground workers (Jenkins and Cullen 1990). However, due to the high productivity of longwall operations, the large zones of full extraction and the intensive mining-induced influence, subsidence impacts of longwall mining operations are experienced more frequently than room-and-pillar operations are. Subsidence results in damage to surface structures, farmland, etc. which are greatly concerned by government, residents, as well as mining corporations (Bian et al. 2012; Xiao et al. 2014; Hu et al. 2015a; Coulson et al. 2017; Ott 2017). Controlling surface subsidence is challenging but significant for sustainable or "green" development of mining industry.

After a longwall panel is extracted the overlying strata are no longer in a state of equilibrium, they collapse with from the immediate roof all the way to the ground surface,

✉ Linfeng Guo
mtkjglf@163.com

1 College of Mining Engineering, Taiyuan University of Technology, Taiyuan 030024, China

2 China National Coal Association, Beijing 100013, China

3 Inner Mongolia Zhengchuang Technology Co., Ltd, Alxa League, China

4 Ordos Rrban Construction Investment Group Co., Ltd, Alxa League, China

5 Inner Mongol Zhongtai Energy Co., Ltd, Alxa League, China

6 Ordos Energy Bureau, Alxa League, China

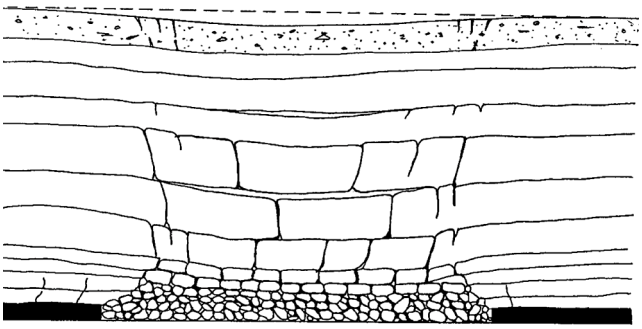

Fig. 1 Schematic for subsidence development (after Peng 2006)

and a depression (or trough subsidence) is developed on the ground surface which covers a large area as shown in Fig. 1 (Esterhuizen et al. 2010; Wang et al. 2017b). However, for conventional longwall mining layout, a gate pillar or chain pillars are left unmined between adjacent panels typically leading to a wavy surface subsidence profile. In addition, due to these pillars between panels, maximum possible subsidence cannot be reached, especially for deep mines, it is referred to as subcritical panels under these conditions as shown in Fig. 2. In most cases, subcritical panels lead to overhang or bridging of overburden rock, and stress arching is developed leading to overstress on the abutment that may result in a gradual deterioration of gate pillar and overburden strata, which may help, eliminate the irregularities and close some of the cracks on the surface. However, in some cases, may lead to instabilities and violent multi-panel collapse failure. In abandoned longwall mines, abrupt secondary or potential subsidence may occur due to the failure of remnant pillars years after extraction (Saeidi et al. 2015). The influence of mining activity on the ground surface is not instant; generally speaking, surface subsidence starts to occur when the mining depth is 2–4 times the mining distance (Hu et al. 2015a). The surface subsidence characteristics of different working face layout are also different (Wang et al. 2023a). It is also very difficult, to predict if or when failure in an abandoned mine might occur. Sometimes overlying strata above abandoned mines may collapse decades after the extraction is finished. The critical width of a panel is the width that needs for the appearance of the maximum possible subsidence at the center of the trough. For the supercritical panel, a flat-bottomed depression will be produced, and the central portion of the trough will attain maximum subsidence. As subsidence is not complete due to the influence of the gate pillar, any damage borne by strata structures is temporary and likely to develop as overburden strata and gate pillars continue to deteriorate, fail and collapse sometime later. Therefore, potential subsidence is of great risk for any future projects on the ground surface above the abandoned mines.

In spite of intensive mining-induced influence, subsidence due to the extraction of longwall panels is delayed. Many case studies have indicated that the ground surface may subside a few days, weeks, months, and in some cases, even years after the face advances past the corresponding surface location. As a result, structures located at the center of the flat-bottomed part of the subsidence trough suffer from the minimum strain.

In fact, the type of structures and deformation that occurs, and whether it influences up to the surface, depends on many factors, such as rock strength, rock type, bulking factor of overlying strata, competence and thickness of overlying beds, mining height, mine depth, mine layout and how far a stratum is over the mined out area. The magnitude, extent, and duration of subsidence can be minimized through effective mine layout, proper barrier and gateroad pillar design, and a rapid and efficient mining system. Many measures being taken to control surface deformation occurred on the surface including backfilling or stowing, planned subsidence, selected extraction, harmonious extraction, simultaneous extraction, limited thickness extraction, etc. (Sui et al. 2015; Zhao et al. 2017).

Split-level longwall layout (SLL) locates gateroads of a longwall panel at different elevations within the same

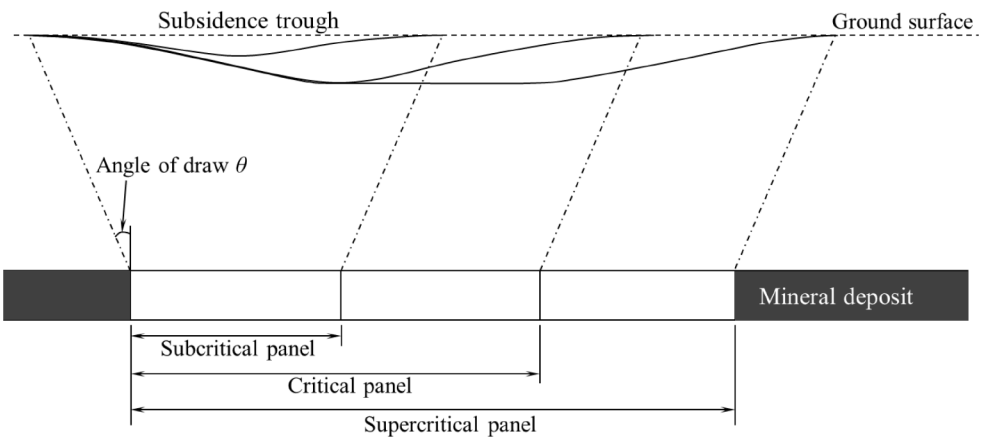

Fig. 2 Panel width and corresponding subsidence profile

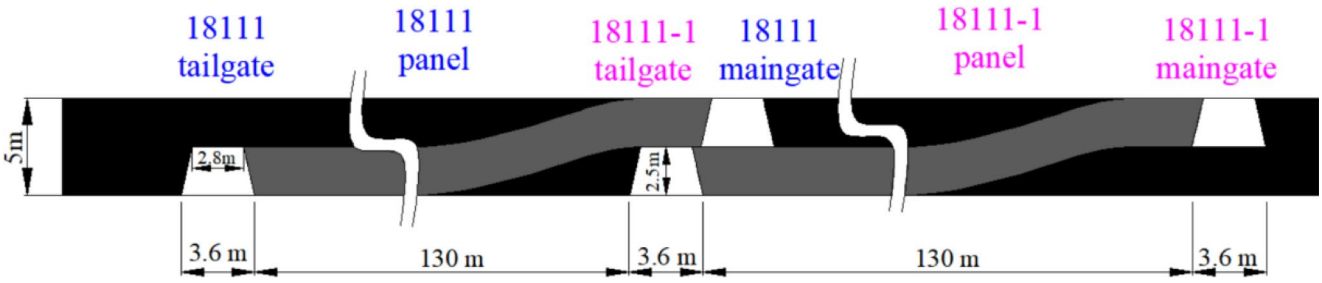

Fig. 3 Split-level longwall layout (SLL)

coal seam. For flat coal seams, the tailgate is excavated immediately on the floor while the headgate is excavated immediately beneath the roof, which gives rise to a gradual elevation in the panel. Depending on field conditions and requirements, this section is elevated by adjusting the inclination of each pan, shield and other mining machines. The tailgate of a panel can be staggered concerning the headgate thus forming an approximate triangular gate pillar. Figure 3 shows SLL for Zhenchengdi coal mine in China (Wang et al. 2017b; Feng et al. 2019; Feng et al. 2019).

Due to the staggered layout of adjacent panels, SLL is preferably adopted for coal seams whose thicknesses are greater than the sum height of two roadways. Since gob needs time to settle, most of times this takes several months to one year to be compacted. Therefore, two adjacent panels must be extracted sequentially, the development of the entry of the future panel should be done at least 6 months (preferably one year) after the previous panel is mined. This point must be kept in mind when a coal mine plans to use the approach. SLL is preferential for coal seams with low gas content or no accumulated gob water. With proper measures, such as pre-drainage of gas through gob wells or cross-measure drill holes, grouting, employing outer offset configuration with a slender pillar in between or leaving a coal sheet between the two adjacent panels then it can be applied for coal seams with higher gas content (Wang et al. 2023a; Wang et al. 2023a). Gob water has to be drained before the adjacent SLL panel is going to be prepared.

Conventional longwall mining system (CLMS) gives rise to wavy subsidence causing great damage to surface structures. Subsidence behavior due to extraction of coal using SLL has never been studied before. It is guessed instinctively that its subsidence behavior must has some advantages over conventional layouts as the gate pillar between adjacent SLL panels is much smaller triangular gate pillar which has little influence on surface subsidence. Therefore, this paper presents a detailed subsidence case study utilizing SLL in coal mine of Shanxi Province, PR China. The study provides an evidence as well as a strong scientific basis for favorable ground subsidence by using SLL.

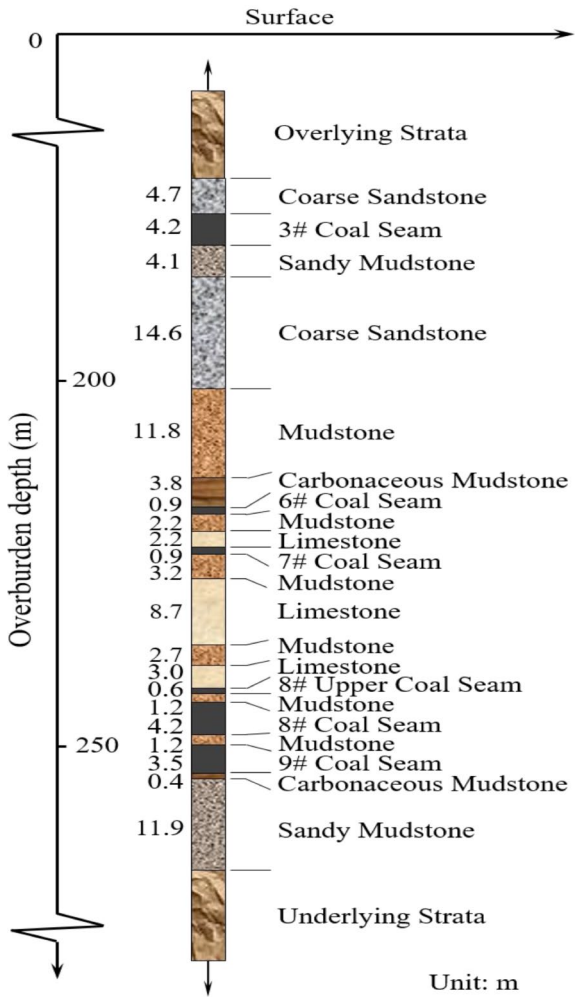

Fig. 4 Generalized stratigraphy column

2 Background

The coal mine for a case study in this paper is situated in the west of Taiyuan, Shanxi Province, PR China. The lithology is dominated by mudstone, limestone and sandstone, as shown in Fig. 4. They are of significantly contrasting mechanical parameters. The No. 8 and 9 coal seams are being mined. No. 8 coal seam is about 4.2 m thick and the No. 9 coal seam is about 3.4 m thick. The burial depth of

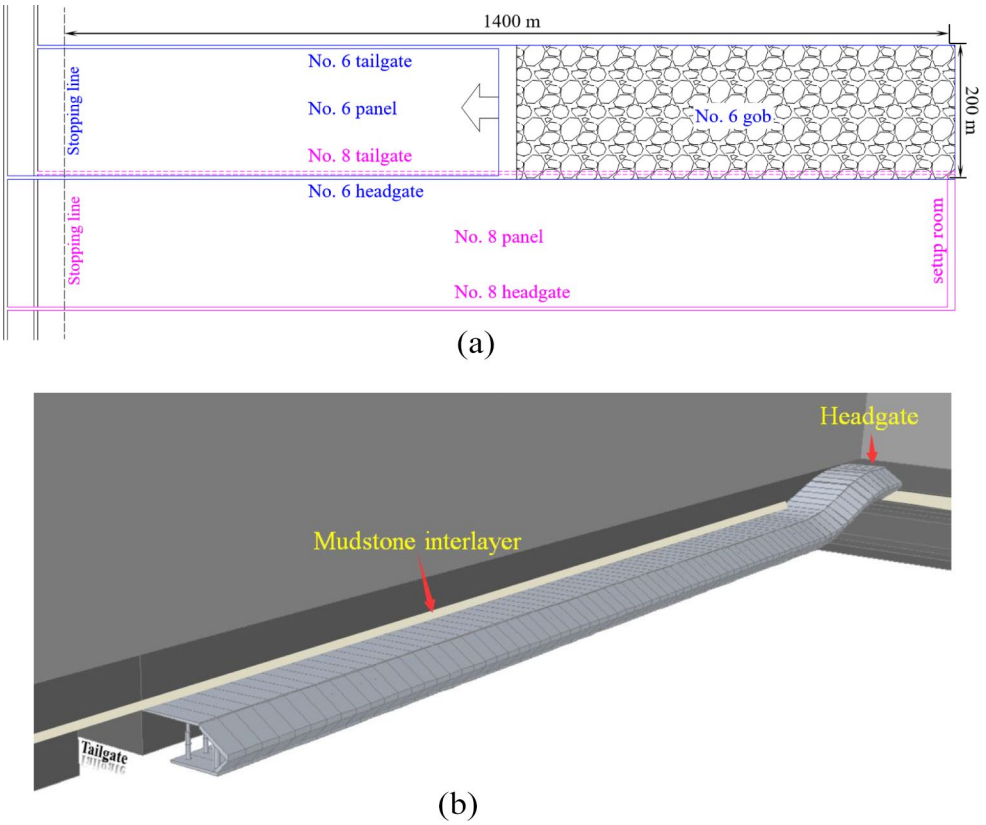

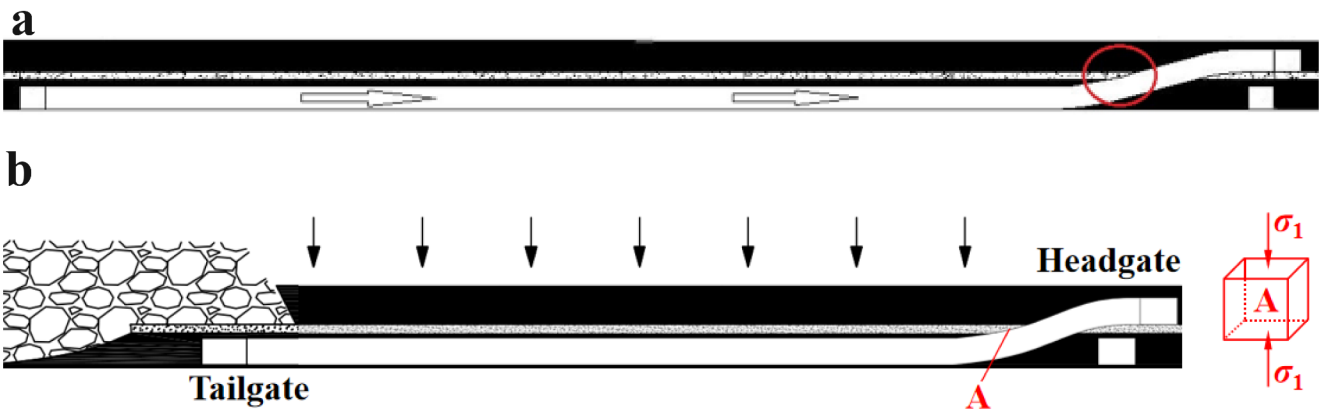

Fig. 5 Split-level longwall layout for No. 6 and No. 8 panels. **a** Plan view of the split-level layout for No. 6 and No. 8 panels **b** 3-D view of the panel

Fig. 6 Geometry of the working face. **a** Configuration of created free space in mudstone interlayer **b** Configuration of created free space in mudstone interlayer

the coal seam is between 200 and 307 m, and the average inclination angle of the coal beds is 8°. The lithology of the No. 8 coal seam roof is mudstone, and the No. 9 coal seam floor lithology is carbonaceous mudstone. There is an interlayer mudstone with an average thickness of 0.8 m between the two coal beds. The mining method in use is longwall top coal caving. As shown in Fig. 5, the SLL method is used to arrange two working faces No. 6 and No. 8 with the same geometric shape. The working faces are 200 m in width and 1400 m in length.

The mudstone interlayer had a significant influence on cavability of top coal due to the inability of the interlayer to cave without delay and large fragmentation of caved mudstone rocks. Previous mining practices show that the large caved mudstone rocks were frequently stuck at the sliding rear canopies when it was open to allow top coal to fall through onto the rear AFC which prevented the top coal above the interlayer from flowing and thus reduced the recovery rate significantly (Feng et al. 2019).

However, for SLL as shown in Fig. 6a, the free space highlighted by the red circle in the working face was created

because SLL panel cut through the mudstone interlayer. The structural model was built correspondingly as shown in Fig. 6b. An infinitesimal was taken from the free surface. As the right side is free, no horizontal force is acting on it, it is only subject to vertical principal stress σ_1 shown in the figure. Therefore, compared with conventional layout, the mudstone interlayer using SLL has smaller caving interval, thus having better caving property that does not affect the top coal caving, flowing or drawing.

2.1 Subsidence measurements

To assess and understand the extent and rate of subsidence, observation stations were installed to collect the subsidence data during the extraction of No. 6 and No. 8 panels, aim to identify potential risks to infrastructure, such as buildings, roads, and pipelines. Two survey lines with monuments spaced at 20 m were laid out including one along the panel centerline in the strike direction and two lines in the dip direction as shown in Fig. 7. Lines 1, 2, 3 are 1000 m in length and extended 300 m out by the panel. Line 4 is 1000 m long as well starting from the center point of the panel and extending to the outer edge that was 300 m away from the panel edge.

There are 51 monuments on these four lines. These monuments were set up before any mining activities were carried out. To be effective, monuments were elaborately constructed making sure that they were not affected by subsidence-unrelated movements, such as soil heave due to freezing, shrinking of surface clay minerals because of rain, etc., and to ensure accurate observations, control conditions must be maintained throughout the monitoring process. These include stable benchmarks or reference points, precise leveling instruments, and regular calibration checks. The working face advanced by around 130 m per month. The extraction of the No. 6 panel was performed from Nov 28, 2015 to Oct 22, 2016. Subsidence observations were made every two months approximately but trying to avoid bad days when rain, snow or fog, etc. occurred. The setup room of the No. 8 panel was ready for working face advance on Mar 5, 2017. On Jun 17, 2017, 450 m of the No. 8 panel was extracted. Therefore, subsidence measurements only on Line 1 and Line 4 were recorded during this period of extraction. One measurement was done on Mar 25, 2017, one on May 5, 2017, and the final time was on June 17, 2017. Due to the period of the observation project, observation contract was over after June 17, 2017, and subsequent subsidence monitoring could not be continued. In addition, despite rigorous control measures, certain uncertainties exist in land subsidence observations. These uncertainties can arise due to natural variations in subsurface geology, variations in groundwater levels, and limitations in measurement techniques. Additionally, external factors such as climate change and human activities may introduce additional complexities and uncertainties into the observed subsidence patterns. Nevertheless, through laborious work of the research group, the data collected were enough for analysis of this research. Subsidence data are plotted as shown in Figs. 8, 9, 10, 11 and 12.

3 Discussion

Figure 8 shows that no subsidence occurred on Line 1 two days after the setup room started to advance (Nov 30, 2015). On Dec 26, 2015, 28 days after the working face departed from the setup room and the working face was around 180 m away from Line 1, the extraction began to influence Line 1 slightly, the maximum subsidence was only 223 mm. On Feb 19, 2016, 9 days after the working face passed by Line

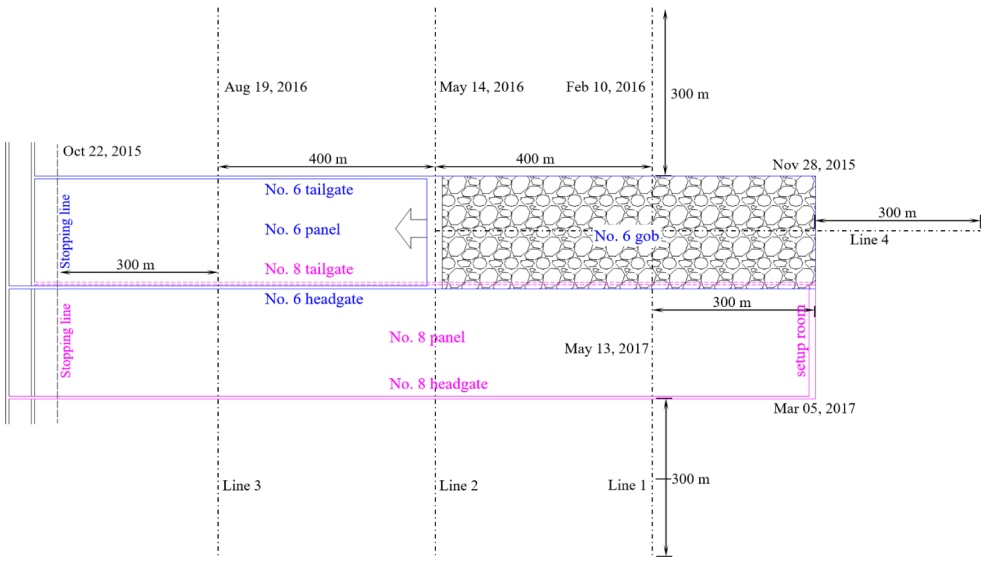

Fig. 7 Survey plan

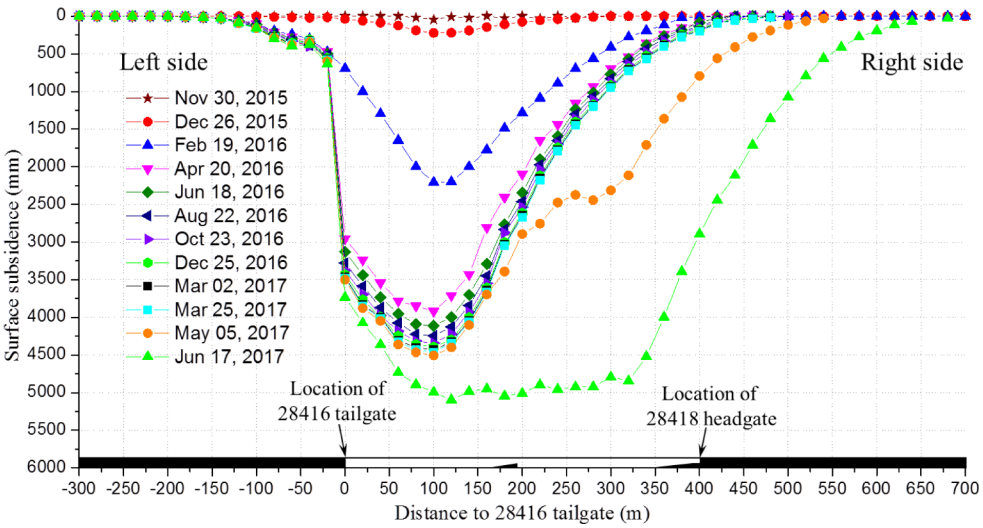

Fig. 8 Subsidence data of Line 1 (Working face reached Line 1 on Feb 10, 2016)

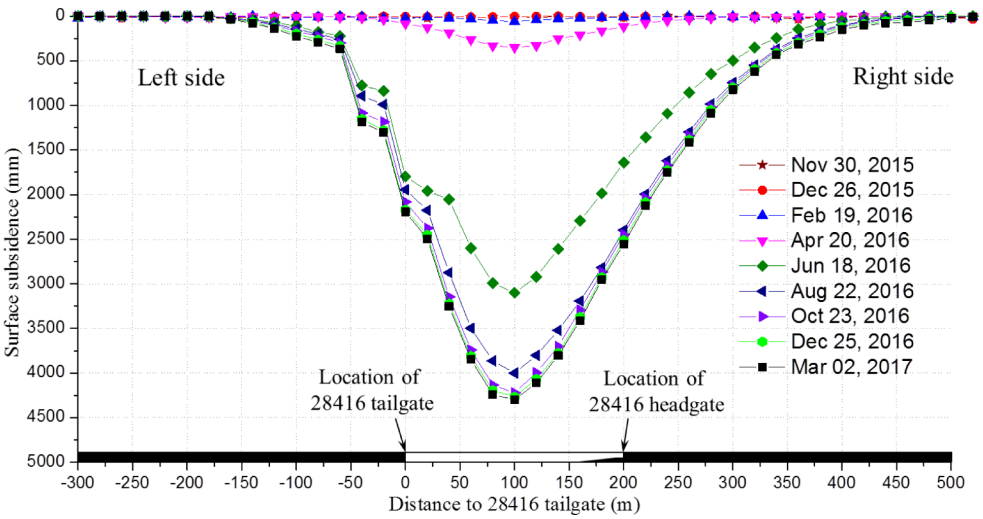

Fig. 9 Subsidence data of Line 2 (Working face reached Line 2 on May 14, 2016)

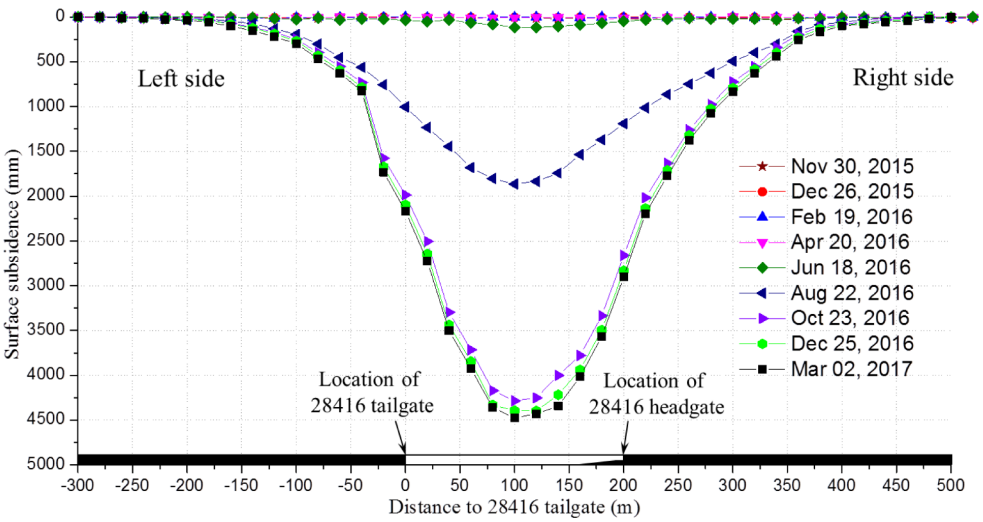

Fig. 10 Subsidence data of Line 3 (Working face reached Line 3 on Aug 19, 2016)

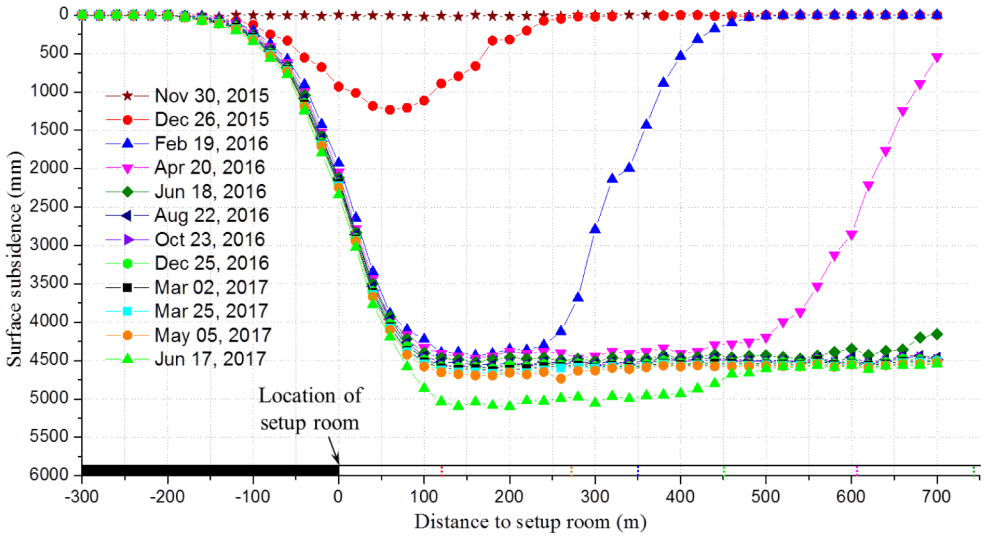

Fig. 11 Subsidence data of Line 4

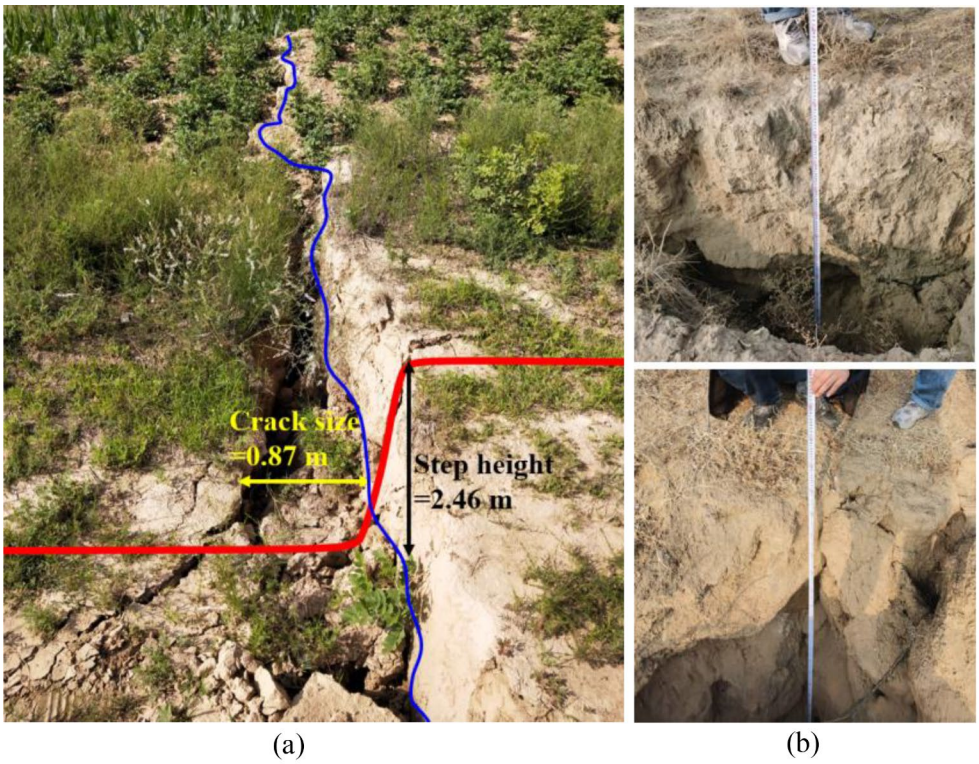

Fig. 12 Stepped subsidence **a** The main crack across Line 1 **b** Cracks at other locations

1, the subsidence grew significantly with maximum subsidence of 2209 mm, but the subsidence profile, the right side in particular, was gentle and smooth, which attributed to the reduction of mining height at the elevating section. On Apr 20, 2016, the subsidence profile shows that an abnormal leap occurred between the points (-20, 343) and (0, 1627), the subsidence value increased abruptly from 475 mm to 2956 mm. This appeared in the form of obvious stepped subsidence and cracks on the surface as shown in Fig. 12. The step was 2.46 m high, and the crack was 0.87 m wide. The configuration is demonstrated in the blue line. This was due to the differential subsidence, shear and tension that caused cracks as the surface stretched over the outer edge of the No. 6 panel. As unconsolidated alluvium, colluvium, and soil cover were not thick enough, stepped subsidence and cracks were not obscured. However, it is hard to predict the exact time when the abrupt stepped subsidence occurred. In this particular case study, it occurred between 10 days to 70 days after the working face advanced past the Line 1. However, on the other side of the No. 6 panel, the subsidence profile remains even and smooth with no sudden increase or leap. This demonstrates that the split-level panel geometry

is conducive to surface structure protection at the elevating section. After Apr 20, 2016, the subsidence kept growing slowly and evenly, which also validates several existing studies indicating that subsidence may completely cease years after panel extraction (Cui et al. 2001). Wang et al. (2017a) also noted that the gob above the elevating section has a lower void ratio and higher compaction or consolidation meaning that the potential or secondary subsidence is less likely to occur.

Overall, since there were no flat-bottomed parts on all curves before Mar 02, 2017, the No. 6 panel is a subcritical panel. Moreover, the asymmetrical panel geometry gave rise to an asymmetrical subsidence profile, and an asymmetrical subsidence trough was developed consequently.

The curves after Mar 02, 2017 were obtained through measurements done on Mar 25, 2017, May 5, 2017 and June 17, 2017. On May 25, 2017, since the working face of the No. 8 panel advanced only 95 m and did not reach the Line 1, the curve was almost the same as that on Mar 02, 2017. Most notably, on May 05, 2017, when the working face was 40 m away from Line 1, the influence of extraction of panel No. 8 was revealed on Line 1. The orange curve indicates that the maximum surface subsidence on Line 1 above the No. 8 panel reached 2438 mm. However, on Jun 17, 2017, when the working face advanced 150 m past Line 1, a flat-bottomed green curve was obtained which means that the width of the extraction in the dip direction was super-critical. This was due to the elimination of the conventional rectangular gate pillar leaving only a tiny triangular pillar that had little effect on surface deformation. In addition, the magnitude of maximum subsidence reached 5096 mm which is larger than that when the width of extraction is subcritical, indicating that the subcritical panel leads to a higher likelihood of potential future subsidence because large voids in the gob of the subcritical panel are not closed even long after extraction. Therefore, future construction projects are more likely to be sound and safe above the abandoned supercritical longwall panels as subsidence is more complete.

It is known that most longwall panels in China are subcritical panels, especially at depth, critical or supercritical width of extraction is much harder to be reached. Potential subsidence is of great risk for future projects on the ground surface above these abandoned coal mines. Therefore, SLL is an alternate measure that can be taken for subsidence control in proper geological settings. If structures can be located at the center of the mined-out area above two or several SLL panels, especially under deep conditions and due to the delayed subsidence, the protection function of SLL for these structures would be better as shown in Fig. 13.

Figure 9 shows that before Feb 19, 2016, no surface subsidence occurred. On Apr 20, 2016, when the working face was 120 m away from Line 2, the surface started to subside slightly. The maximum on Line 2 was only 348 mm. On June 18, 2016, 35 days after the working face passed by Line 2, the corresponding curve shows that evidently stepped subsidence occurred twice on the left side of the panel on the ground surface. The maximum subsidence reached 3102 mm. It is only certain that the stepped subsidence on Line 2 occurred between Apr 20, 2016 and Jun 18, 2016, which indicates that the stepped subsidence may occur after or before the working face reached Line 2. By contrast, the right side of the profile suggests that the subsidence on the right of the panel was mild and uniformly continuous which is also attributed to the elevated geometry on the right side of the panel.

Data on Aug 22, 2016 (Three months after the working face advanced past Line 2) shows that the subsidence got certain mild and even increase compared with subsidence on Jun 18. 2016. The maximum subsidence was 3984 mm. Data on Oct 23, 2016 suggests that there was a small amount of subsidence increase compared with subsidence on Aug 22, 2016. The subsidence curves since Oct 23, 2016

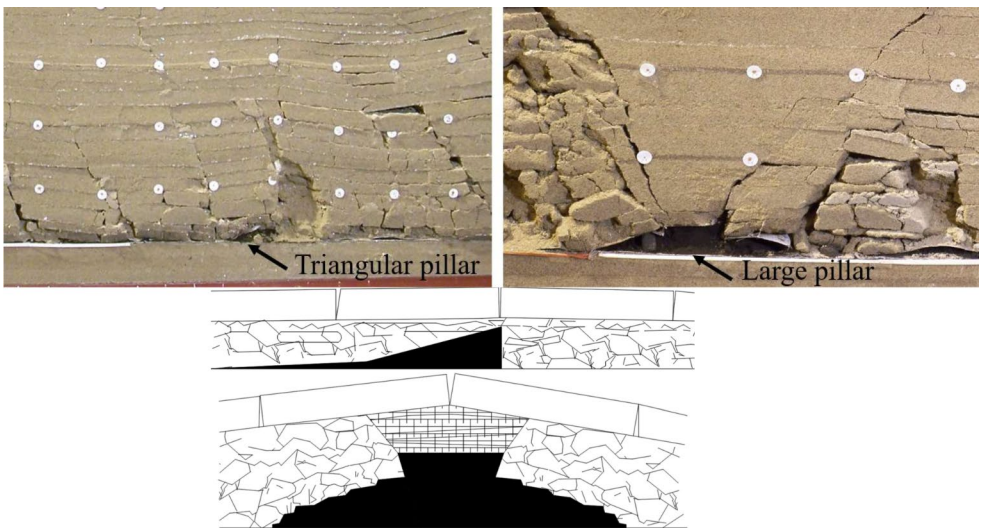

Fig. 13 Characteristics of the subsidence employing SLL and CLMS (Wang et al. 2014)

indicate that the subsidence kept increasing but very slightly and subsidence may almost cease.

Figure 10 shows that no subsidence occurred before Apr 20, 2016. On Jun 18, 2018, when the working face was 250 m away from Line 3, a very tiny subsidence that was hard to be detected by the naked eye occurred, which could only be seen by a sophisticated and accurate survey instruments. On Aug 22, 2016 when the working face passed by Line 3 for three days, the maximum subsidence reached 1864 mm yet smooth without any sudden leaps. On Oct 23, 2016, two months after the working face passed by Line 3, the subsidence increased significantly with a magnitude of maximum subsidence of 4384 mm. Although there was no evident stepped subsidence, the subsidence profile was not even smooth. Unlike the disorder or differential of the left part of the profile, the right side of the subsidence curve was still mild and uniformly continuous. After that, the subsidence increased very slowly. The last time of measurement (Mar 02, 2017) indicates that the maximum subsidence on Line 3 was 4664 mm.

Figure 11 shows that no surface subsidence occurred on Nov 30, 2015. On Dec 26, 2015, when the working face was about 120 m away from the setup room, the subsidence on Line 4 showed that it did not get critical or super-critical width of extraction, and the magnitude of the maximum subsidence was 1234 mm. On Feb 19, 2016, when the working face was about 350 m away from the setup room, however, it shows that the width of extraction was supercritical in the strike direction since a flat-bottomed curve was observed and the magnitude of the maximum subsidence reached 4435 mm. However, the width of extraction in the dip direction was still subcritical. From Feb 19, 2016 on and before May 05, 2017, lengths of flat-bottomed parts on subsequent curves increased with the advance of the working face and the subsidence still kept growing but very slowly. The curve on Jun 17, 2017, the working face of the No. 8 panel advanced 150 m past Line 1, overlying strata above No. 6 and the No. 8 gobs subsided together, two panels acted as one supercritical panel, and the maximum magnitude of subsidence on Line 1 increased to 5097 mm. As No. 8 panel was extracted only 450 m when the project ended, survey points whose coordinates were larger than 450 hardly changed. This also demonstrates that the isolated troughs are ultimately joined together due to the supercritical size reached for multiple SLL panels.

3.1 Numerical modeling

The ground surface subsidence was further analyzed by the Universal Distinct Element Code (UDEC) and the final parameters are given in Tables 1 and 2. Two models were established to investigate the difference in surface subsidence between the SLL and the CLMS with 20 m of gate pillar. Both two models were built 1000 m long and 340 m high, and the Coulomb-Moore model was used as a constitutive model, the bottoms of the models were fixed in both two directions, the left and right sides were fixed in the horizontal direction, and the vertical direction was free. The in-situ stress varying with depth was applied inside the model, and the in-situ stress gradient was 20 kPa/m. And the strata structure of the overlying strata was simplified for the efficiency of calculation, some strata that are too thin were grouped with the adjacent thick stratum. As the coal seam is near horizontal, the dip angle is small, less than 8°, so the dip angle of the numerical model is set to be 0°. To prevent the model from being unable to reach equilibrium due to disorderly vibration at the equilibrium position, viscous damping is applied using the damp auto command. This damping exerts a force in the opposite direction of the block's motion velocity. The force is proportional to the block's motion velocity, thus speeding up the model's equilibrium velocity without affecting the results. The parameters of each stratum in the model were obtained by laboratory testing on drill core samples supplemented by data provided by other researchers. The model is shown in Fig. 14. The numerical simulation process was as follows: after the model was established, the in-situ stress gradient and gravity acceleration were applied first, and the model was iterated to reach the initial equilibrium state. Then, the first panel is simulated to be excavated and calculated to equilibrium, and the subsequent panel is excavated and calculated to equilibrium. Since the migration of overlying strata is small before the main roof is not broken, it has little influence on the surface subsidence, so the working face was excavated at one time.

After the models were established, both models simulate the extraction of the model in two steps to simulate the successive extraction of two panels. After each extraction, models were calculated to equilibrium, And a survey line was set up in the loess layer to monitor the surface subsidence. The models after two extractions and balance are shown in Fig. 15, and the comparison of the subsidence curve with the measured curve is shown in Figs. 16 and 17.

Figures 16 and 17 show that the simulated subsidence range of the surface subsidence curves after two equilibria are smaller than the field data. The reason is that the overlying No. 2, 3 and 6 coal seams have been mined before the field measurement, and the gobs of the overlying No. 2, 3, and 6 panels are not completely collocated with the panels in No. 8 and 9 in the vertical direction. Therefore, when the No. 8 and 9 coal seams were mined, the overlying key stratum of the lowest No. 6 coal seam that has been mined was already influenced by mining. The key stratum was full of fractures, so the subsidence range was larger. This phenomenon was also proved by Dong (2020) and Wang (2013).

Table 1 The parameters for each stratum in the model (Jia 2020)

Lithology	Thickness (m)	Density (g/cm^3)	Cohesion (MPa)	Friction angle (°)	Tensile strength (MPa)	Bulk modulus (GPa)	Shear modulus (GPa)
Loess	24.0	1820	0.02	20.2	0.015	0.3	0.1
Sandy mudstone	14.0	2410	2.5	35.1	2.4	4.24	2.19
Medium-grained sandstone	15.0	2813	8.3	38	2.7	25.71	16.17
Mudstone	6.5	2340	1.2	30	0.5	6.55	2.02
Fine-grained sandstone	26.0	2408	3.2	42	1.2	26.11	12.75
Sandy mudstone	24.0	2465	2.4	39	1.9	4.57	2.48
Fine-grained sandstone	4.0	2518	3.5	40	1.5	24.65	14.09
Siltstone	22.0	2540	2.2	36	0.9	3.99	2.17
Medium-grained sandstone	4.0	2780	7.7	38	2.5	26.94	15.40
Sandy mudstone	28.0	2300	2.4	30	1.1	4.68	2.29
No. 2 Coal Seam	2.8	1390	0.8	30	1.5	5.00	2.05
Coarse sandstone	4.6	2350	4.0	35	2.0	20.00	12.00
No. 3 Coal Seam	4.2	1410	0.8	31	1.5	5.19	2.12
Mudstone	4.1	2150	1.0	30	0.5	6.67	1.43
Coarse sandstone	14.6	2590	11.6	40.8	3.1	19.43	13.97
Sandy mudstone	15.6	2250	2.5	35	1.5	3.85	2.42
No. 6 Coal Seam	3.0	1390	0.8	30	1.5	4.50	2.08
Carbonaceous mudstone	8.5	2390	2.3	35	1.4	4.17	2.15
Limestone	8.7	2550	13.0	40	13.0	13.33	10.00
Mudstone	2.7	2200	7.0	27	2.5	9.77	7.02
Limestone	3.0	2720	15.5	44	11.5	21.67	16.25
Carbonaceous mudstone	1.8	2060	2.01	16	1.5	3.10	1.30
No. 8 Coal Seam	5.4	1380	0.8	30	1.5	4.67	2.15
No. 9 Coal Seam	3.5	1230	1.3	18	2.1	10.25	4.73
Sandy Mudstone	20.0	2350	3.9	39	1.2	17.33	10.40
Sandstone	70.0	2500	25.0	30	5.0	16.7	10.0

Table 2 The parameters for joint in the model

Joint type	Normal stiffness (Pa)	Shear stiffness (Pa)	Friction angle (°)	Cohesion (Pa)	Tensile strength (Pa)
Mudstone - Losses	1.00×10^7	4.00×10^6	17	0.00	0.00
Mudstone - Mudstone	2.80×10^8	9.00×10^7	27	6.00×10^5	4.00×10^5
Sandstone - Sandstone	2.01×10^9	8.40×10^8	28	1.90×10^6	1.90×10^6
Sandstone -Coalseam	9.50×10^8	3.80×10^8	18	1.10×10^6	6.00×10^5
Mudstone - Coalseam	2.80×10^9	9.00×10^7	27	6.00×10^5	4.00×10^5
Mudstone - Limestone	2.80×10^9	9.00×10^7	27	6.00×10^5	4.00×10^5

But the gob of No. 2, 3 and 6 panels were not considered in this numerical modeling due to lack of information.

It is also noted that the subsidence after extraction of one panel is also much smaller than the field measurement. This may be because the width of the panel is far less than the critical width of extraction in the dip direction in numerical simulation. A huge bed separation with a maximum height of 3 m and a length of 70 m appears under the overlying competent stratum as shown in Fig. 18. In practice, after the extraction of the upper No. 2, 3 and 6 coal seams, the competent stratum that is not expected to have been fractured after the extraction of one panel was fractured, so the field-measured surface subsidence was about 3 m larger than the simulated maximum subsidence.

What's more, no flat-bottomed trough appeared after the extraction of one panel, indicating that the surface subsidence had not fully developed due to the extraction of only one panel. Figure 17 shows a flat-bottomed trough that appeared after the extraction of two panels, meaning that the width of the two panels was supercritical. This can be further illustrated by comparing the extraction of SLL panels with CLMS panels.

Figures 19 and 20 are the surface subsidence curves after the extraction of two SLL panels and two CLMS panels, respectively. Figure 19 shows that after the extraction of one panel, the maximum subsidence values of the two methods are similar. The maximum subsidence of the CLMS is 1047 mm, and that of the SLL is 1111 mm. The difference between the CLMS and SLL is only 64 mm.

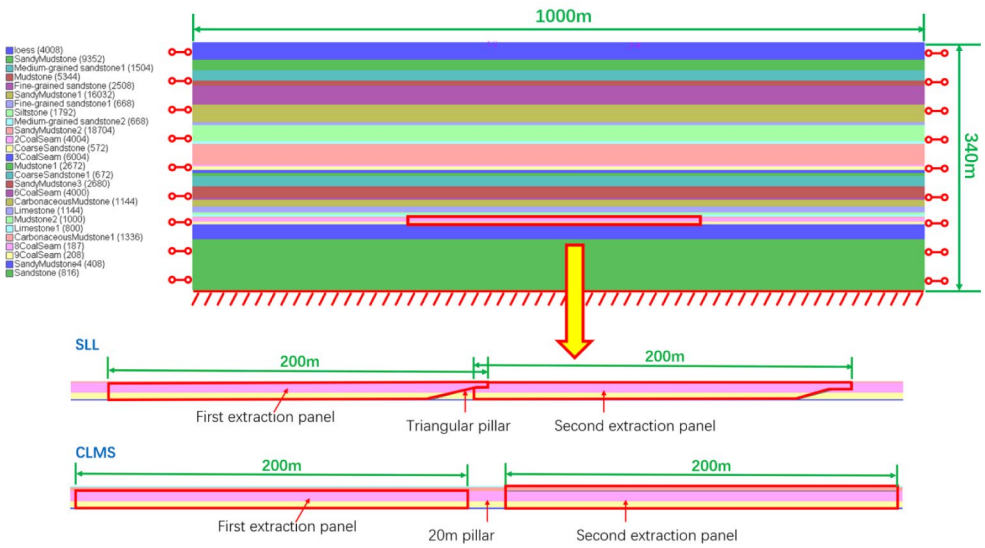

Fig. 14 The UDEC model built

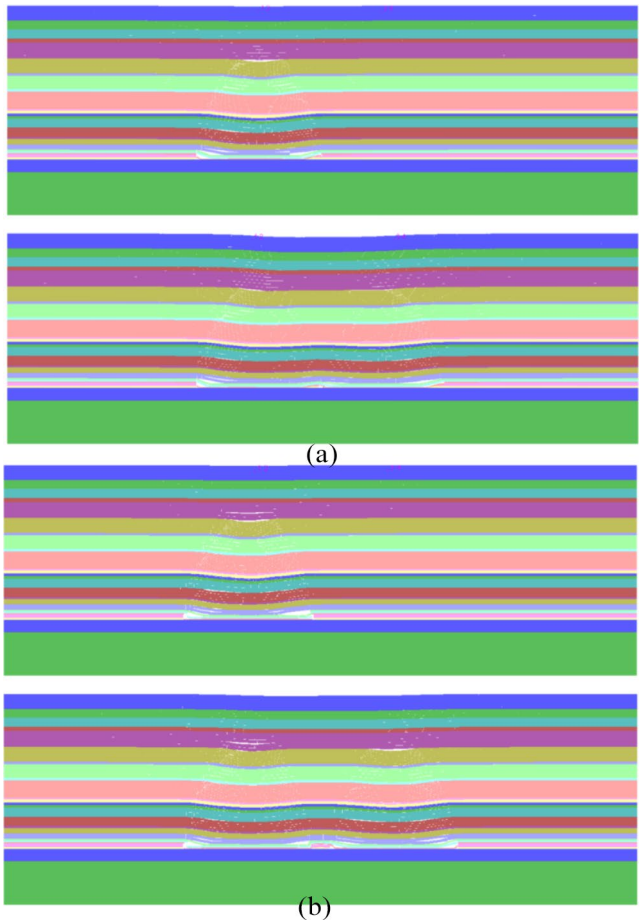

Fig. 15 The models after extractions. **a** SLL **b** CLMS

After the extraction of two panels, however, the maximum subsidence of the CLMS is 3349 mm, while the maximum subsidence of the SLL reaches 5777 mm. The evident difference is as large as 2428 mm. This also proves again through numerical simulation that the small triangular pillar developed by using SLL has little influence on strata movement. And part of the caved zone above the first panel and the caved zone above the successive panel connected, which leads to the expansion of caving strata downward during the extraction of the successive panel. Therefore, the SLL gob is more compact. In other words, the long-term stability of SLL gob is better. Figure 18 shows that for SLL, the right side of the large separation mentioned above is basically closed while the left side is still open which proves above point of view. Figure 21 is the joints with zero normal force and shear force export from UDEC, as shown in Fig. 21, a large number of fractures formed during the first extraction are reduced or closed. Therefore, it can be concluded that after the extraction of the second SLL panel, the width is supercritical. However, for CLMS, a conventional large coal pillar separated the two adjacent panels, so the extraction of the second CLMS panel has a very limited effect on rock strata above the first CLMS panel. In Fig. 18, unclosed separations are still visible for CLMS.

As shown in Fig. 22, the exported images of UDEC were post-processed to obtain the model outline. By exporting the UDEC block to CAD, the Boolean operation is carried out in CAD to delete closed cracks, so the area of outer contour, block and subsidence could easily get. Then the area of fracture could be obtained by subtracting the area of block after extractions from the area of outer contour after extractions, the area of expansion are calculated by subtracting the area of block before equilibrium from the area of block after extractions, these data are shown in Table 2.

The difference between SLL and CLMS is further compared by calculating the fracture rate, which is the percentage of the fracture volume in the mined coal volume, which is simplified to the percentage of the fracture area in the mined area under two-dimensional conditions, so the calculation formula of the fracture ratio is as follows:

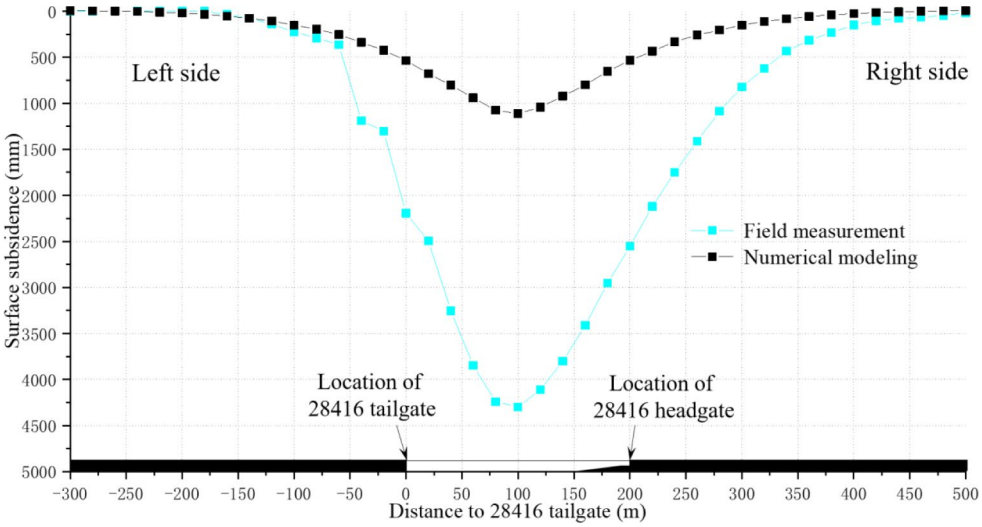

Fig. 16 Comparison of the subsidence curve of numerical modeling with the measured curve after extraction of one panel

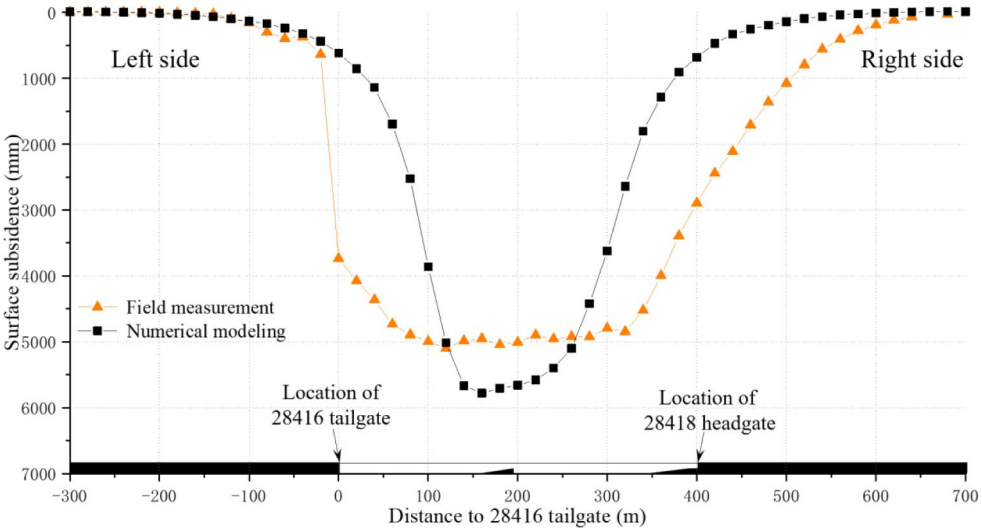

Fig. 17 Comparison of the subsidence curve of numerical modeling with the measured curve after extraction of two panels

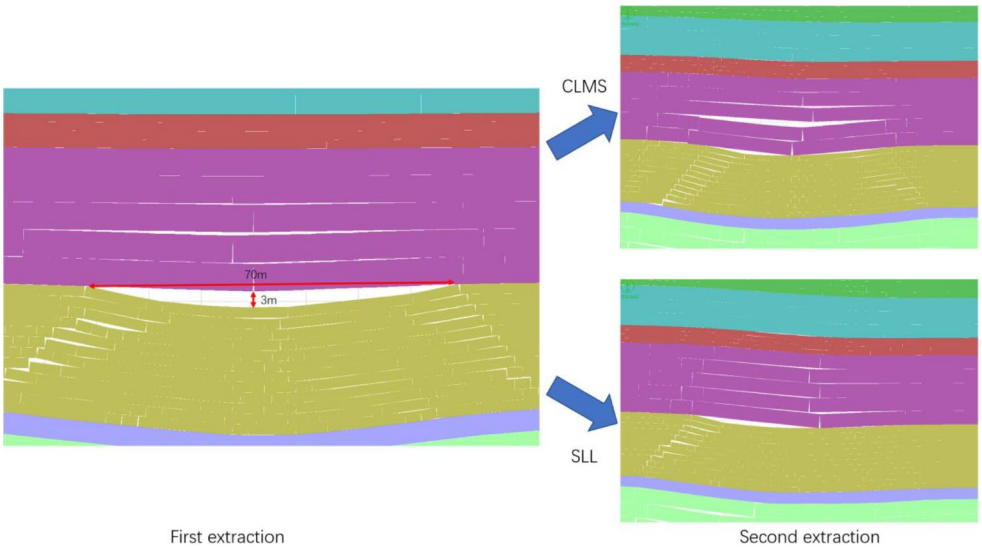

Fig. 18 Changes of separation

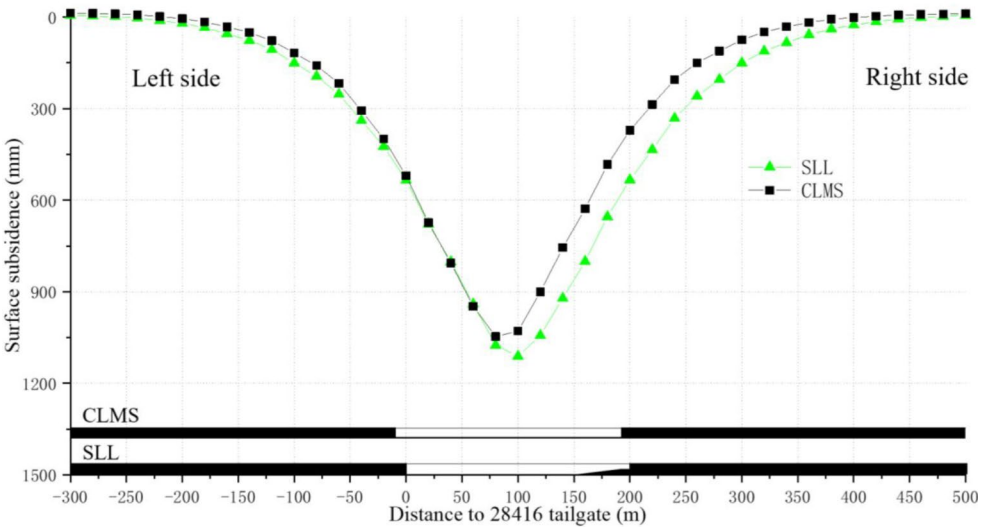

Fig. 19 Comparison of the surface subsidence curve with SLL and CLMS after the first equilibrium

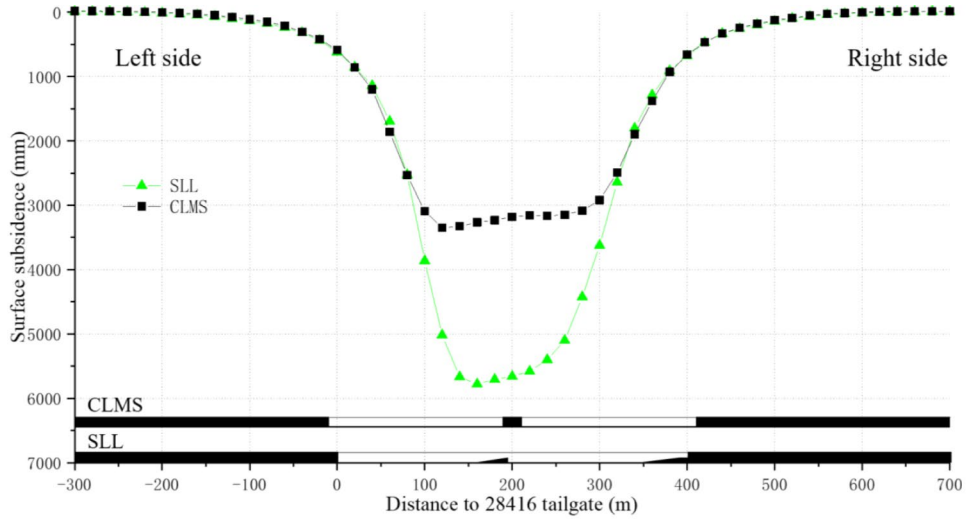

Fig. 20 Comparison of the surface subsidence curve with SLL and CLMS after the second equilibrium

$$R_f = \frac{V_f}{V_g}$$

Among them, R_f is the fracture ratio; V_f is the fracture area, the area of fracture of SLL is V_{fs}=1805.116 m^2, the area of fracture of CLMS is V_{fc}=2507.378 m^2; V_g is the area of coal mining, and the area of coal mining of SLL is V_{gs}=393×8.9 -7×5.9-7×3=3435.4 m^2, the area of coal mining of CLMS is V_{gc}=400×8.9=3560 m^2.

So the fracture rate of SLL is R_{fs}=52.54%, and that of CLMS is R_f=70.43%. It can be seen that CLMS has 17.89% more fractures than SLL. These fractures may close slowly in the later residual subsidence process, causing secondary damage to the surface upon CLMS gob.

In addition the area of block expansion of SLL is 2342.7782 m^2 smaller than it of CLMS, and the area of subsidence of SLL is 413.0622 m^2 larger than it of CLMS as shown in Table 3, which indicated that blocks have much more space to migration under condition of SLL than CLMS. The blocks of CLMS were forced to deform due to the lack of migration space, further causing the instability of the underground space of CLMS condition.

The ground fissures of SLL can also be studied in Fig. 22. According to statistics data as shown in Table 4, there are 18 ground fissures with an opening of more than 9 cm above the ground, including 10 ground fissures on the left side of the gob center and 8 ground fissures on the other side of the gob center. The reason for the uneven distribution of ground fissures is that there is a gentle slope on the right side of the gob, which cause the subsidence of the right side is more gentle, so SLL will cause more damage on the left side of the gob center than the right side.

Figure 20 shows that after the extraction of the second panel, the subsidence curves of CLMS also have a flat-bottomed section, but from the above analysis, the separations above CLMS gob are still not closed, and the subsidence is

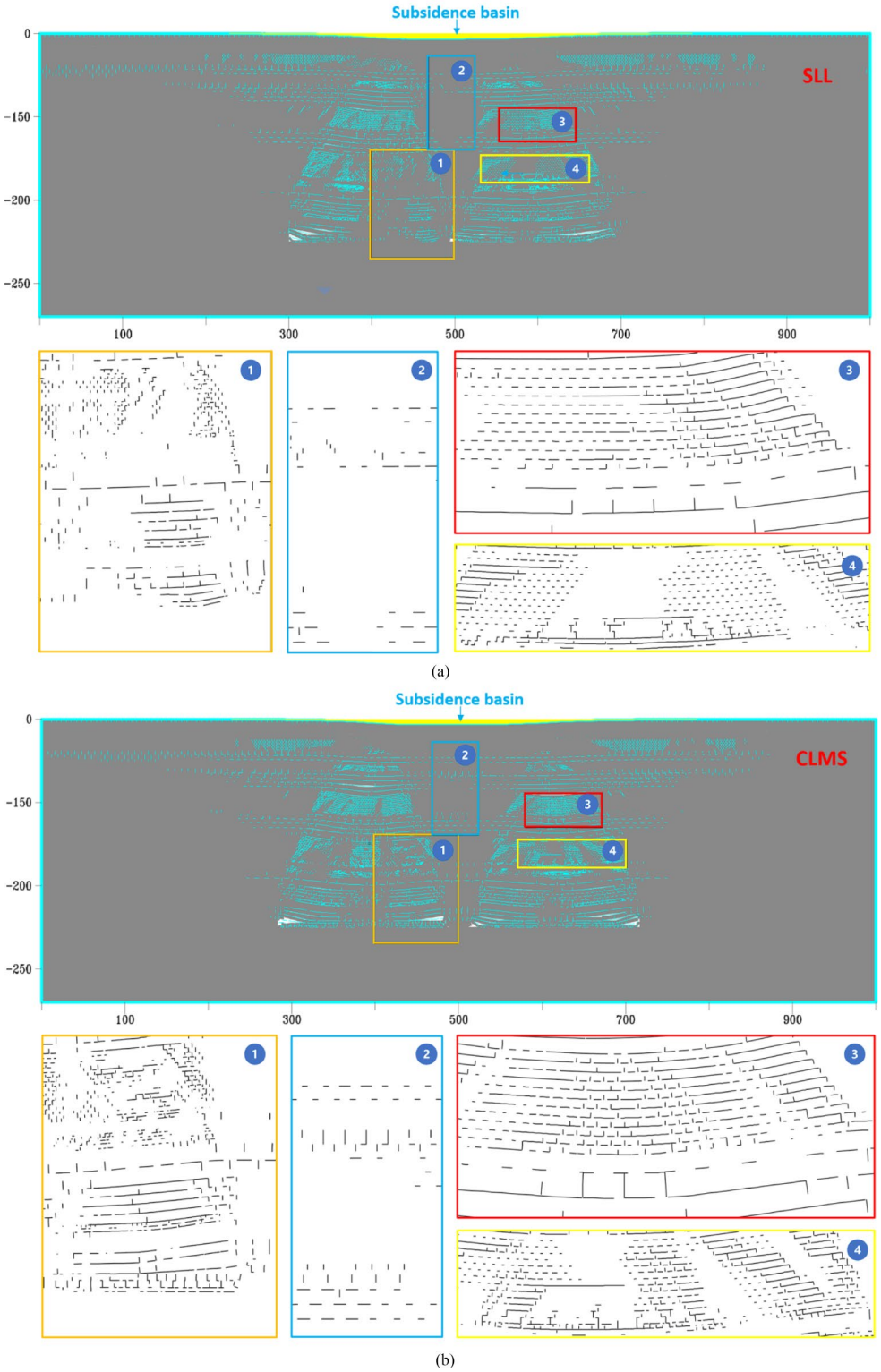

Fig. 21 Comparison of the fractures with SLL and CLMS after the second equilibrium. **a** SLL **b** CLMS

small. However, the separation in the strata above the SLL gob is basically closed, and the subsidence is larger. Therefore, in the dip direction, whether the subsidence curve has a flat-bottomed or near flat-bottomed section cannot be the criterion for judging the critical width of extraction.

4 Conclusions

(1) Every individual longwall panel was subcritical and maximum possible subsidence could not be reached,

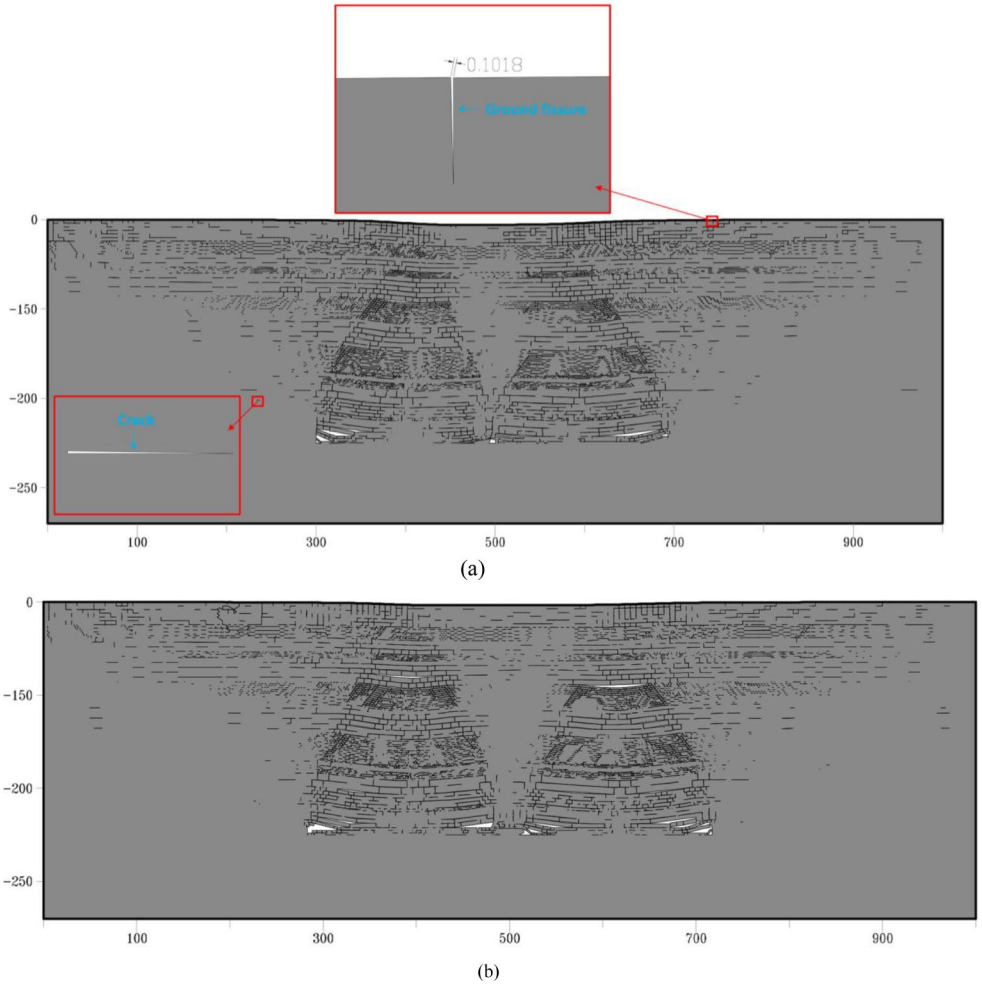

Fig. 22 The model outline. **a** SLL **b** CLMS

Table 3 Comparison of the area data with SLL and CLMS

Method	Area of Fracture (m^2)	Area of Outer contour (m^2)	Area of Block after extractions (m^2)	Area of Subsidence (m^2)	Area of block expansion (m^2)
SLL	1805.1160	338436.8160	336631.7	1563.1840	67.1
CLMS	2507.3782	338849.8782	336342.5	1150.1218	2409.8782

Table 4 Statistics data of ground fissures of SLL

Number	Distance to subsidence center	Fracture aperture	Number	Distance to subsidence center	Fracture aperture
1	-336.9942	0.1002	10	-126.0484	0.1005
2	-270.8922	0.1003	11	177.9161	0.1018
3	-228.7906	0.1	12	190.0104	0.1015
4	-210.6301	0.0999	13	202.0982	0.1011
5	-192.6148	0.1001	14	226.3435	0.1006
6	-174.49	0.1	15	244.47	0.0997
7	-156.4016	0.1001	16	268.5301	0.1007
8	-144.2314	0.1002	17	298.6441	0.1005
9	-138.2082	0.1006	18	418.81	0.1

future potential subsidence is of great risk for any projects on the ground surface as large voids in the gob of subcritical panel are not closed even long after extraction.

(2) SLL with asymmetrical panel geometry led to asymmetrical subsidence with stepped subsidence and cracks on the tailgate side but relatively mild and smooth subsidence on the other.

(3) Due to the conventional rectangular gate pillar, overlying strata above No. 6 and No. 8 gobs subsided together, two panels acted as one supercritical panel. The width of the extraction in the dip direction was super-critical, maximum possible subsidence was reached and subsidence is more complete with a higher degree of gob consolidation. The likelihood of potential future secondary subsidence is minimal as underground gob fractures and voids close.

Overall, SLL is more favorable for post-mining land reuse as gobs are more consolidated underground. This study is applicable for coal mines utilizing longwall mining, especially for those using SLL. But please not that the findings of this paper are not totally applicable for all the other mining projects. Because geologic conditions are different. For instance, a number of coal mines using SLL are mining coal seams with large inclination such as Tangshan, Huafeng, Hebi, Gongwusu, Jingyuan Huating, etc. The subsidence results of these longwall panels must be different from the case presented in this manuscript as the coal seam in this case is relatively flat. So the subsidence of using SLL for coal seams with large dip angle need further studies. The mining subsidence behavior is also site specific. For similar geologic conditions and mining layout present in this paper, the mining subsidence behavior can be similar but with slight variation depending on overlying strata characteristics.

Acknowledgements The authors extend special thanks to coal mine leaders' cooperation during the field observation and measurements.

Author contributions P.F. Wang, L.F. Guo, Z. Zhu and H.X. Wang proposed the ideas and main contents of the research; Z. Zhu performed numerical modelling analysis; P.F. Wang, L.F. Guo, Z. Zhu and H.X. Wang performed the data analyses and wrote the manuscript; P.F. Wang, L.F. Guo, Yue Qu, Yaoxiong Zhang, Linwei Wang, Hua Wang revised the manuscript.

Funding This study was funded by the General Program of the National Natural Science Foundation of China (52274092), Hu-Bao-E National Independent Innovation Demonstration Zone Construction Science and Technology Support Project (2023XM08) and Funds for Talents Supported by the China Association for Science and Technology (YESS20200211).

Data availability Data and materials are available from the corresponding author on reasonable request.

Declarations

Competing interests The authors declare no conflict of interest.

References

Bian ZF, Miao X, Lei S, Chen S, Wang W (2012) The challenges of reusing mining and mineral-processing wastes. Science 337(6095):702–703

Coulson N, Ledwaba P, McCallum A (2017) Building resilient company- community relationships: a preliminary observation of the thoughts and experiences of community relations practitioners across Africa. 117(1):7–12The Journal of the Southern Africa Institute of Mining and Metallurgy

Cui X, Wang J, Liu Y (2001) Prediction of progressive surface subsidence above longwall coal mining using a time function. Int J Rock Mech Min Sci 38(7):1057–1063

Dong CC (2020) Research on overburden rock and surface Movement and deformation under repeated mining, (Master). Taiyuan University of Technology, Available from Cnki

Esterhuizen E, Mark C, Murphy M (2010) Numerical model calibration for simulation coal pillars, gob and overburden response. In: Proceeding of the 29th international conference on ground control in mining, Morgantown, WV: West Virginia University. pp. 46–57

Feng G, Wang P (2019) Stress environment of entry driven along gob-side through numerical simulation incorporating the angle of break. Int J Min Sci Technol 2019. https://doi.org/10.1016/j.ijmst.2019.03.003

Feng GR, Wang PF, Chugh P, Zhao JL, Wang ZQ A New Gob-side Entry Layout for Longwall Top Coal Caving. Energies. 11(5): 1292., Ghabraie B, Ren G, Zhang XY, Smith J (2018) 2015. Physical modelling of subsidence from sequential extraction of partially overlapping longwall panels and study of substrata movement characteristics. Int. J. Coal Geol, vol. 140, pp. 71–83

Feng GR, Wang PF, Chugh P (2019) Stability of the Gateroad Next to an Irregular Yield Pillar: A Case Study. Rock Mechanics and Rock Engineering, 2019, 52(8): 2741–2760. https://doi.org/10.1007/s00603-018-1533-y

Hu Z, Fu Y, Xiao W et al (2015) Ecological restoration plan for abandoned underground coal mine site in Eastern China. Int J Min Reclam Environ 29(4):316–330

Hu QF, Deng XB, Feng RM, Li CY, Wang XJ, Tong J (2015a) Model for calculating the parameter of the Knothe time function based on angle of full subsidence, vol 78. International Journal of Rock Mechanics & Mining Sciences, pp 19–26

Jenkins FM, Cullen ET (1990) Review of single-entry longwall mining technology in the United States. Pgh. [Pittsburgh]. U.S. Dept. of the Interior, Bureau of Mines, PA

Jia Y (2020) Analysis and prediction of influencing factors of mining ground fractures in Guandi mining area, (Master). Taiyuan University of Technology, Available from Cnki

Lee DK, Mojtabai N, Lee HB, Song WK (2013) Assessment of the influencing factors on subsidence at abandoned coal mines in South Korea. Environ Earth Sci 68(3):647–654

Malinowska Agnieszka, Cui Ximin, Salmi Fathi Ebrahim, Hejmanowski Ryszard (2022) A novel fuzzy approach to gas pipeline risk assessment under influence of ground movement. Int J Coal Sci Technol 9(1): 47. https://doi.org/10.1007/s40789-022-00511-2

Maria Przyłucka, Zbigniew Kowalski, Zbigniew Perski (2022) Twenty years of coal mining-induced subsidence in the Upper Silesia in Poland identified using InSAR. Int J Coal Sci Technol 9(1): 86. https://doi.org/10.1007/s40789-022-00541-w

Ott T (2017) Finding the interface between mining, people, and biodiversity: a case study at Richards Bay Minerals. The Journal of the Southern Africa Institute of Mining and Metallurgy, vol. 117, no. 1. pp. 1–5

Peng SS (2006) Longwall mining, second edition. West Virginia University, Department of Mining Engineering, Morgantown, WV

Peng SS, Ma WM, Zhong WL (1992) Surface subsidence engineering. Society for Mining, Metallurgy and Exploration. Littleton, Colorado

Qiao J (2014) Julia Sets and Complex Singularities of Free Energies. Memoirs of the American Mathematical Society, vol. 234, no. 1102. pp. 1

Saeidi A, Deck O, Heib MA, Verdel T (2015) Development of a damage simulator for the probabilistic assessment of building vulnerability in subsidence areas. Int J Rock Mech Min Sci 73:42–53

Sahu P, Lokhande RD (2015) An investigation of sinkhole subsidence and its preventive measures in underground coal mining. Procedia Earth Planet Sci 11:63–75

Sui W, Zhang D, Cui ZC et al (2015) Environmental implications of mitigating overburden failure and subsidences using paste-like backfill mining: a case study. Int J Min Reclam Environ 29(6):521–543

Wang YX (2013) Study on regularity of surface subsidence due to repeated mining taking Daliuta Coal Mine as example. (Master), China University of Mining and Technology, Available from Cnki

Wang ZQ, Guo XF, Gao Y, Chen CF, Li PF, Wang L, Zhao JL (2014) Study of grouting technology of overburden- separation to reduce ground subsidence in huafeng coal mine. Chin J Rock Mechan Eng 33(s1):3249–3255

Wang H, Zhang D, Wang X, Zhang W (2017a) Visual exploration of the Spatiotemporal Evolution Law of overburden failure and Mining-Induced fractures: a case study of the Wangjialing Coal Mine in China. Minerals 7, pp 35

Wang PF, Zhao JL, Wang ZQ, Sun ZW, Xu CH, Song ZY, Su Y (2017b) Mechanism of gob-pillar interaction for subcritical panels and its application. Chin J Rock Mechan Eng 36(5):1185–1200

Wang P, Chang T, Lu J (2023) Re-discussion on reasonable position and support technoloay of entry driven under the gob edge of previous split-level longwal panel. J China Coal Soc 48(02):593–608. https://doi.org/10.13225/j.cnki.jccs.2022.1599

Wang P, Liu J, Feng G (2023a) Stress distribution and failure characteristics of a longwall panel floor with a negative gate pillar. Chin J Rock Mechan Eng 42(1):194–211. https://doi.org/10.13722/j.cnki.jrme.2022.0189

Wang P, Niu Y, Chen K Field survey on the evolution of main ground cracks under condition of forced hard roof caving in mining ultra-thick coal seams under shallow overburden. J China Coal Soc. 2023,:1–17https://doi.org/10.13225/j.cnki.jccs.2022.1651

Xiao W, Hu Z, Chugh YP et al (2014) Dynamic subsidence simulation and topsoil removal strategy in high groundwater table and underground coal mining area: a case study in Shandong Province. Int J Min Reclam Environ 28(4):250–263

Zhao JL, Wang PF, Su Y (2017) An innovative longwall mining technology in Tangshan coal mine, China. Minerals 7:pp14